CHEMISTRY
A EUROPEAN JOURNAL

DOI: 10.1002/chem.201100318

Yolk-Shell Gold Nanoparticles as Model Materials for Support-Effect Studies in Heterogeneous Catalysis: Au, @C and Au, @ZrO_2 for CO Oxidation as an Example

Carolina Galeano,[a] Robert Güttel,[a] Michael Paul,[a] Pablo Arnal,[b] An-Hui Lu,[c] and Ferdi Schüth*[a]

Abstract: The use of nanostructured yolk-shell materials offers a way to discriminate support and particle-size effects for mechanistic studies in heterogeneous catalysis. Herein, gold yolk-shell materials have been synthesized and used as model catalysts for the investigation of support effects in CO oxidation. Carbon has been selected as catalytically inert support to study the intrinsic activity of the gold nanoparticles, and for comparison, zirconia has been used as oxidic support. Au, @C materials have been synthesized through nanocasting using two different nonporous-core@mesoporous-shell exotemplates: Au@SiO_2@ZrO_2 and Au@SiO_2@*m*-SiO_2. The catalytic activity of Au, @C with a gold core of about 14 nm has been evaluated and compared with Au, @ZrO_2 of the same gold core size. The strong positive effect of metal oxide as support material on the activity of gold has been proved. Additionally, size effects were investigated using carbon as support to determine only the contribution of the nanoparticle size on the catalytic activity of gold. Therefore, Au, @C with a gold core of about 7 nm was studied showing a less pronounced positive effect on the activity than the metal oxide support effect.

Keywords: carbon · co-oxidation · gold · nanocasting · yolk-shell materials

Introduction

Yolk-shell materials have recently attracted interest due to their particular optical,[1] catalytic,[2] and electrochemical[3] properties. Importantly, this kind of materials combine high thermal stability with monodisperse and narrow particle-size distributions,[2a,b,d] characteristics that make them very interesting for heterogeneous catalysis. These characteristics are not only interesting from an application point of view, but can also reduce complexity for kinetic and mechanistic investigations. In tailored yolk-shell catalysts, the catalytic properties of the entire catalyst are very homogeneous with little variation from active particle to active particle. Thus, the resulting catalytic activity of the system can directly be associated to the structure of the model particle, and not as an average of all possible morphologies like in traditional solid catalysts. In particular, in such yolk-shell materials all catalytic particles have identical size, and the contact with the support is similar for each particle. These aspects make yolk-shell materials powerful model systems for support and size-effect studies.

During the last decades, gold has been an interesting active material for several reactions depending on the catalyst support.[4] For CO oxidation, gold nanoparticles supported on metal oxides have emerged as one of the best catalysts.[5] Despite the unique properties of gold catalysts, it is still far from being completely understood how they exactly work. While the role of gold nanoparticles to adsorb CO molecules on low coordinated Au atoms is generally accepted,[6] the role of the support is not clear yet, although it is known to be crucial for the catalytic activity. One model assumes the activation of oxygen by adsorption on reducible metal–oxide supports and its transfer to the metal-support interface, where the reaction takes place.[7] Another model proposes that the number of low coordinated Au atoms is the governing the factor of adsorption of both CO and O_2 and thus for the activity.[6] The support would then indirectly influence activity by inducing different concentrations of active sites on the gold. A comparison of supported and unsupported gold catalyst would be desirable, to give insight into the role of the support. However, the catalytic activity

[a] C. Galeano, Dr. R. Güttel, Dr. M. Paul, Prof. F. Schüth
Department of Heterogeneous Catalysis
Max-Planck Institut für Kohlenforschung
Kaiser-Wilhelm-Platz 1, 45470 Mülheim an der Ruhr (Germany)
Fax: (+49) 208-306-2995
E-mail: schueth@mpi-muelheim.mpi.de

[b] Dr. P. Arnal
Centro de Tecnología de Recursos Minerales y Cerámica (CETMIC)
Cno. Centenario y 506, C.C.49 (B 1897 ZCA)
M. B. Gonnet. Pcia. de Buenos Aires (Argentina)

[c] Prof. A.-H. Lu
State Key Laboratory of Fine Chemicals
School of Chemical Engineering
Dalian University of Technology
116024 Dalian (P.R. China)

Supporting information for this article is available on the WWW under http://dx.doi.org/10.1002/chem.201100318.

of unsupported gold nanoparticles has not deeply been studied for comparable systems. The published approaches rely on nanoporous gold[8] and gold powder.[5] However, the comparability is limited, because gold catalysts are very sensitive to the preparation method and to the size of the gold particle.[5,9] Additionally, gold is one of the metals with the lowest melting point and thus sintering of metal nanoparticles becomes a crucial problem at elevated temperatures,[10] leading to a reduced catalytic activity. This hampers the investigation of activity of unsupported gold nanoparticles. In this work, we have synthesized Au, @C through nanocasting, to obtain sinter stable gold nanoparticles supported on carbon that is considered to be catalytically rather inert. This provides insight in how much the support determines the activity of gold in CO oxidation. Carbon can be considered the base case for a non-interacting support.

The synthesis of carbon encapsulated gold nanoparticles was already presented by Kim et al.[11] The authors describe the covering of gold nanoparticles with a nonporous–mesoporous double silica shell, which can subsequently be used as exotemplate for nanocasting of the mesoporous carbon shell. However, neither the thermal stability nor catalytic tests of this material were reported. Our strategy for the synthesis of the Au, @C material is based on our previous standard synthesis procedure for the Au, @ZrO_2 yolk-shell material.[2b] It combines the encapsulation of gold nanoparticles in a binary nonporous-silica mesoporous-zirconia exotemplate, which is further used for the nanocasting of the carbon shell.[12] The obtained Au, @C material would allow the investigation of the activity of gold nanoparticles not supported on metal oxides. Thus, the effect of oxidic supports on the activity of gold in CO oxidation can be quantified without the danger of sintering and superimposed particle-size effects. First, we discuss the resulting textural properties and high-temperature stability of the Au, @C material. Furthermore, the activity of Au, @C nanoparticles in CO oxidation has been investigated and compared with the standard Au, @ZrO_2 material. Additionally, also the effect of the size of the gold nanoparticle has been investigated, combining our ex-post size reduction strategy[13] and the encapsulation in carbon.

The synthesis method, following a bottom-up strategy, is shown in Figure 1. First, a silica covered gold colloid (Au@SiO_2) is prepared as already discussed elsewhere (step i).[2b,11] Subsequently, the material is covered with a mesoporous shell (MS) from either zirconia or silica (step ii) denoted as zirconia and silica route, respectively. The covering by a mesoporous shell of zirconia is described elsewhere.[2b] The mesoporous silica shell formation follows the method proposed by Büchel et al.,[14] that consists of the reaction of a mixture of TEOS and *n*-octadecyltrimethoxysilane (OTMS). The resulting exotemplate (diameter ca. 100 nm) is used for the nanocasting of the carbon shell, which is based on polymerization of furfuryl alcohol inside the pores of the mesoporous shell (step iii). Afterwards, the polyfurfuryl alcohol (PFA) composite is carbonized under argon (step iv). Finally, the exotemplate is removed by treatment with NaOH or HF (step v) yielding gold nanoparticles encapsulated in hollow mesoporous carbon spheres. The ex-post size reduction is carried out after the step i. Basically, the Au@SiO_2 is aged in water and afterwards the gold core is partially dissolved by the treatment with a leaching agent as reported elsewhere.[13] We have used sodium cyanide as leaching agent with the stoichiometry chosen according to the target size. After, this step the process follows the same path as described in Figure 1.

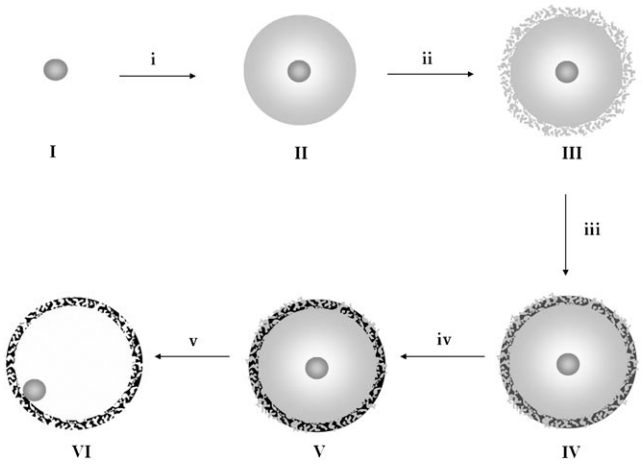

Figure 1. Scheme of the synthesis pathway to Au, @C yolk-shell materials. I) Gold colloid. II) Silica covered gold nanoparticles Au@SiO_2. III) Exotemplate Au@SiO_2@MS (MS = ZrO_2 or *m*-SiO_2). IV) Polymer composite material Au@SiO_2@MS,P. V) Carbon composite material Au@SiO_2@MS,C. VI) Yolk-shell material Au, @C.

Results and Discussion

Figure 2 shows the evolution of the materials during the removal of the exotemplates. After treatment of Au@SiO_2@ZrO_2,C (Figure 2a) with aqueous NaOH, the siliceous core is selectively removed, releasing the gold nanoparticle inside the ZrO_2,C composite cage (Figure 2b). The subsequent treatment with HF removes the zirconia shell leading to the final Au, @C (Figure 2c) system. Similarly, the final Au, @C material for the silica route (Figure 2e) was obtained by treatment of the carbon composite (Figure 2d) with NaOH. For both routes, well-separated gold nanoparticles of (13.8 ± 0.2) nm entrapped in monodisperse carbon spheres were obtained. It was observed that some agglomeration of the carbon shells occurs during the nanocasting step. However, since the Au nanoparticles are effectively separated from each other by a carbon shell, this agglomeration is not considered a problem in catalytic applications. The Au, @C materials exhibit carbon shell thicknesses of about (9.0 ± 0.3) and (12.8 ± 0.7) nm for the zirconia and silica route, respectively. However, the shell thickness can be increased by addition of higher amounts of the respective precursors. It is also possible to tune the gold core size by a controlled post-encapsulation leaching step.[13] As an exam-

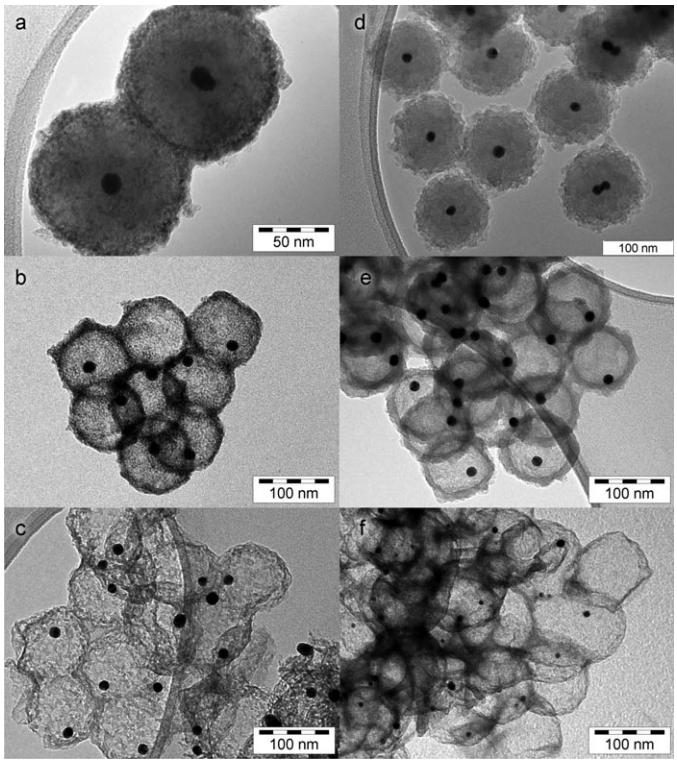

Figure 2. TEM images of the intermediate and final materials. a)–c), f) Zirconia route. d)–e) Silica route. a) Carbon composite material Au@-SiO_2@ZrO_2,C. b) Yolk-shell composite Au, @ZrO_2,C. c) Yolk-shell Au, @C 14 nm gold core from zirconia route. d) Carbon composite material Au@SiO_2@*m*-SiO_2,C. e) Yolk-shell Au, @C 14 nm gold core from silica route. f) Yolk-shell Au, @C 7 nm gold core from zirconia route.

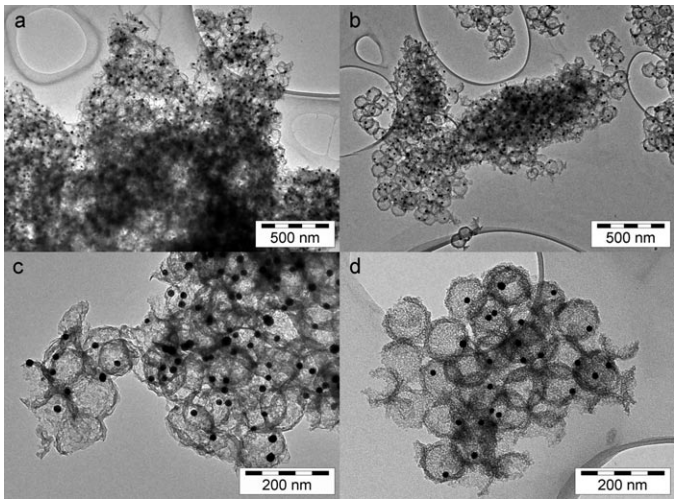

Figure 3. TEM images of Au, @C material after thermal treatment at 900 °C for 3 h under argon. a, b) Zirconia route. c), d) Silica route.

ple, Au, @C with a gold core size of 7.2 ± 0.2 nm was prepared (Figure 2 f). Due to the ex-post manner of core size reduction, this material has a reduced gold content per yolk-shell particle. However, for catalytic comparison the number of gold nanoparticles within the entire catalyst sample remains almost constant, which was taken as comparison basis.

In order to test the thermal stability, the final materials were heated with a rate of 2 K min^{-1} to 900 °C under argon and subsequently compared to the as made materials by TEM (Figure 3). The materials obtained via the silica route are stable during this treatment with respect to the shell integrity and sintering of the gold cores. This is less obvious for the materials obtained with the zirconia template shell. This material exhibits a thinner carbon shell, and a higher fraction of broken spheres was already observed in the as made material. Nevertheless, in spite of the presence of broken shells, significant agglomeration of the gold nanoparticles was not observed. Further improvement of the shell thickness will lead to higher quality of the material, providing improved thermal stability. However, the coalescence of the gold nanoparticles was indeed prevented during thermal treatment at 900 °C under argon (Figure 3 a and b). Since carbon reacts with oxygen, the thermal treatment had to be carried out under protective atmosphere, and such catalysts would only be suitable for high-temperature reactions under reducing conditions. The stability of the carbon shell in air was investigated by TGA, showing thermal stability up to about 350 °C (Figure S1 in the Supporting Information).

In addition to the TEM studies, the final and intermediate products were characterized by XRD and nitrogen sorption measurements. The XRD results are shown in Figure S2 in the Supporting Information). It was observed, that the zirconia shell is composed by grains, which build a porous network. The zirconia crystallite size of (2.4 ± 0.7) nm was calculated with the Whole Pattern Powder Modelling method (WPPM)[15] from the (101) reflection (ca. 30° 2θ). Elemental composition of the intermediate materials and final materials was investigated by EDX (Table S1 in the Supporting Information).

The evolution of the pore structure of the materials, from both the zirconia and silica route, was investigated by nitrogen physisorption measurements (Figure 4 and Table S1 in the Supporting Information). The pore-size distribution was calculated by the BJH method. Both exotemplates (material III, Figure 1) show a type IV adsorption isotherm typical for mesoporous materials. The pore volume of the material from the silica route is higher than that of the solid resulting from the zirconia route. This can be explained by the bigger pores and the thicker mesoporous silica shell. In contrast, after the filling of the pore system with the polymer, the porosity of the composite materials (Au@SiO_2@MS,PFA) is reduced for both routes towards similar pore volumes (for $p/p_0 < 0.9$). During carbonization, microporosity is generated due to shrinkage of the polymer. The resulting type I isotherms of the carbon composites (material IV, Figure 1) show a similar behavior for both routes, with a slightly higher pore volume for the silica route. The slight difference can be explained by an increased shrinkage of the higher polymer volume (due to higher pore volume) for the silica route during carbonization.

The removal of the silica core in the zirconia route leads to only a slightly increased nitrogen uptake (material Au,

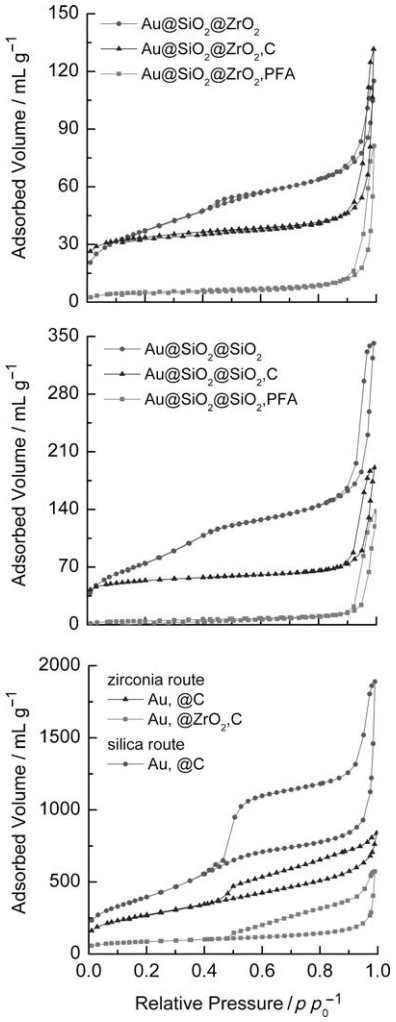

Figure 4. Nitrogen sorption isotherms of exotemplate and composite material before carbonization for the zirconia (top) and silica (middle) route; (bottom) composite material after partial and complete exotemplate removal.

@ZrO_2,C). This may be explained by the fact, that the removal of the nonporous silica core introduces no additional micro- and mesoporosity into the material, except the internal surface of the spherical shell. The hysteresis between adsorption and desorption branch is consistent with the yolk-shell structure of the material.[16] It can be attributed to the space inside the spheres that is accessible by window pores in the shell. The desorption branch of the Au, @ZrO_2,C material shows a step at a relative pressure of about 0.48, which could suggest a narrow pore-size distribution at about 4 nm according to BJH model. However, as the zirconia shell is filled with carbon, mesopores of about 4 nm are not expected, since the pore size of the exotemplate is between 2.7 and 3.7 nm. As consequence, this step should probably not be attributed to the presence of mesopores with 4 nm size. It is rather due to filling of internal voids by nitrogen at high pressure. These inside voids can only be emptied through narrow pores in the shells, and this occurs at a pressure where the meniscus becomes unstable, which is also known as critical instability of the meniscus or as the Tensile Strength Effect (TSE).[17]

Further removal of the zirconia from the ZrO_2,C composite shell leads to a significant increase of the pore volume and thus in nitrogen uptake. This is caused by the porosity opened up in the remaining C matrix during removal of the zirconia grains. The desorption branch of the isotherm of the final Au, @C material shows the same drop at relative pressure of about 0.45, but steeper. In this case, the presence of mesopores cannot be discarded completely by considering the TSE. Taking into account that the grain size of ZrO_2 in the exotemplate is about 2.4 nm, after its removal pore sizes around this value may be formed in the carbon replica after zirconia removal. However, also the TSE may partially be responsible for this drop, which is suggested by the position of the desorption step at a relative pressure close to $p/p_0 =$ 0.42. A reliable pore size can thus not be extracted from these sorption data. The sorption isotherm of the Au, @C material from the silica route shows significantly higher nitrogen uptake compared to the zirconia route (Figure 4). The higher mass fraction of polymer in the composite would lead to increased shrinkage of the polymer during carbonization and thus to increased porosity. The broad hysteresis loop with a long plateau and a prominent steep step in the desorption branch at relative pressures of about 0.46 is due to emptying of the internal void through the narrow pores in the shell. This effect is most pronounced for the Au, @C material from the silica route, in line with the TEM observations. Such an isotherm is expected for a sample consisting of fully intact shells, which is found by TEM in this sample (Figure 2e). The materials obtained from the zirconia route contain a significant fraction of defective spheres for which no intact internal void exists and thus a more conventional sorption isotherm is expected.

Catalytic investigation: Figure 5 shows the results of the catalytic tests for oxidation of carbon monoxide as a model re-

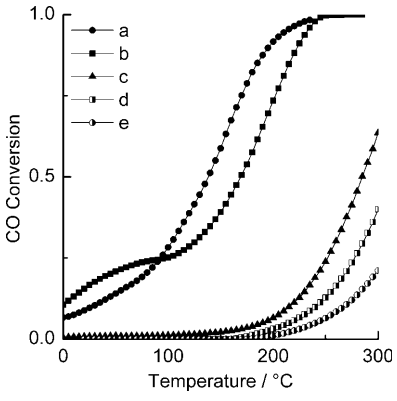

Figure 5. Conversion-temperature curves for CO oxidation on different materials (a–d: Au core = 14 nm). a) Au, @ZrO_2. b) Au, @ZrO_2,C. c) Au, @C silica route. d) Au, @C zirconia route. e) Au, @C zirconia route (Au core = 7 nm). 50 mg of catalyst in a gas mixture of 1% CO in air. Flow rate of 67 $cm^3 min^{-1}$ corresponding to a space velocity of 80 000 $cm^3 h^{-1} g_{cat}^{-1}$.

action. Comparison of the activity of the already known Au, @ZrO_2 system and the composite yolk-shell material Au, @ZrO_2,C shows similar activity normalized to the Au, @ZrO_2 mass. The carbon thus only adds weight to the system without further influencing the catalytic activity. Incidentally, this also means that the gold nanoparticles can be reached without diffusion limitation even across the composite ZrO_2,C shell. If mass transfer limitations were present, the composite shell with the smaller pores would lead to lower catalytic activity. Since this is not observed, mass transfer limitations can be excluded for these samples.

In contrast to the catalytic performance of the composite samples, the activity of the materials based on pure carbon supports is much lower. The half conversion temperature obtained for the Au, @C material is much higher (315 °C) than for the Au, @ZrO_2 material. The activity of the carbon-based catalysts is at least one order of magnitude lower than that of the oxide-based systems. Thus, carbon as a support material does lead to catalysts with low activity. The activity observed here may in fact be the intrinsic activity of the gold nanoparticles without positive influence from a support. To rule out the deactivation of the gold from F^- ions during the zirconia removal by HF, the Au, @C material obtained via the silica route was also investigated by catalytic measurements. In line, also for this material the activity was rather low with a half conversion temperature of 285 °C. This difference between both routes is relatively small, and thus significant deactivation by the HF treatment can be excluded.

Furthermore, the pronounced difference in half conversion temperature between Au, @C, and the corresponding Au, @ZrO_2 material proves the strong effect of the oxidic support in the catalytic activity of gold for the CO oxidation. For investigation of the particle-size effect, catalytic measurements were also conducted for the Au, @C obtained via the zirconia route with a Au core diameter of about 7 nm. $T_{50\%}$ for this material was slightly higher than for the corresponding 14 nm Au, @C materials. The Au, @C material of 7 nm core presents a lower gold content and overall smaller gold surface area (roughly by a factor of four), however the number of particles is kept ideally constant in both catalyst. The activity of the 7 nm core material is by about a factor of two higher than for the 14 nm material. Although the size effect is visible, it is not comparable with the effect of oxidic supports instead of carbon, which improves the activity dramatically even for gold particle sizes above 5 nm. The findings of this study thus strongly support the published proposals that there is a strong synergistic effect between the gold nanoparticles size and the nature of the support for activity in CO oxidation.[9]

Conclusion

The nanocasting/sacrificial templating method presented in this paper offers the possibility to prepare sinter-stable carbon supported gold catalysts. Two different exotemplates are presented for production of well separated gold nanoparticles inside spherical carbon shells. Yolk-shell materials are not only interesting from the material synthesis point of view, but also are highly attractive for mechanistic studies. This was demonstrated for the study of the effect of oxidic supports in gold catalyzed CO oxidation. Oxidic supports always have a decidedly positive effect on activity, even for zirconia as relatively inactive support. An additional interesting feature of our results is the possibility to prepare a composite shell from carbon and transition-metal oxides without mass-transfer limitations in the reaction tested. This can open a way to new applications, like for instance bifunctional supported catalysts. The functionalization of the carbon or the oxidic surface could be attractive for many applications. Since both educts and products have to pass the shell, this could improve the catalyst performance. For example, a functionalized shell could eliminate catalyst poisons or refine the products when passing the shell, leading to improved selectivity towards the intended product. Furthermore, the presented approach could also be applied to other core materials.

Experimental Section

Au@SiO_2@ZrO_2 exotemplate preparation: This material is prepared according to our previous protocol.[2b]

Au@SiO_2@*m*-SiO_2 exotemplate preparation: The exotemplate preparation is based on literature information.[2b] Specifically, an aqueous ammonia solution (3.29 mL, 28–30 %) was mixed with absolute ethanol (65.33 g) in a 100 mL flask first. Then the Au@SiO_2 colloid, prepared as described elsewhere,[2b] was dispersed in 6.6 g of millipore water and added to the ammonia solution. The flask was sealed with a septum and stirred at room temperature for 30 min. Afterwards, a mixture of TEOS and octadecyltrimethoxysilane (OTMS) (1.08 mL TEOS, 0.44 mL OTMS) was added dropwise within 20 min. The molar ratio of the mixture TEOS/OTMS was fixed at 4.7. After the addition of the precursors, the stirring was stopped and the system was allowed to react for 6 h. Subsequently, the solvent was removed by centrifugation (8000 rpm; 10 min) and the product was dried at 70 °C overnight. Finally, the material was calcined in air by heating the system with a heating rate of 2 K min^{-1} from room temperature to 550 °C followed by natural cooling to room temperature.

Carbon composite preparation: The synthesis of both composites consists basically of four steps. In the first step, the exotemplates (Au@SiO_2@ZrO_2, Au@SiO_2@*m*-SiO_2) were evacuated under vacuum at 250 °C overnight to remove adsorbates from the porous material, and subsequently kept under argon for 30 min. Afterwards, the pore volume, determined by nitrogen sorption, was filled with a mixture of monomer (FA, furfuryl alcohol, liquid at ambient conditions, 98 %) and catalyst (oxalic acid, anhydrous, 98 %) via the incipient wetness method (FA/catalyst: 100/1). The FA/catalyst solution was added dropwise in three steps under vigorous shaking by hand. During this infiltration, the solid was forcefully crushed with a spatula against the internal wall of the glass flask for about 10 min. The monomers inside the pore system were left to diffuse at 50 °C for 24 h. Afterwards, the system was heated to 90 °C for 24 h under air to allow the polymerization of the monomer. Finally, the polymer was thermally carbonized under argon by heating the sample with a heating rate of 5 K min^{-1} to 850 °C and kept at the final temperature for 3 h.

Removal of the exotemplates: The siliceous part of the exotemplate was removed by treatment of the composite with NaOH (1 M) for 24 h under stirring at 50 °C and the zirconia was removed by the treatment of the

material with stoichiometric amounts HF (40% in water) for 6 h at room temperature. The final material was washed five times with water and once with absolute ethanol by centrifugation (9000 rpm; 15 min) and dried overnight at 70 °C.

Ex-post size reduction: This material was prepared according to our previous protocol.[13]

Catalytic test: The activities of the catalysts for the oxidation of CO were measured in a plug-flow reactor using 50 mg of catalyst in a gas mixture of 1% CO in air (from Air Liquide, 99.997% purity) at a flow rate of 67 $cm^3 min^{-1}$, which corresponds to a space velocity of 80 000 $cm^3 h^{-1} g_{cat}^{-1}$.

Acknowledgements

Funding by the DFG (SFB 558) is gratefully acknowledged. We thank B. Spliethoff and A. Dreier for TEM analysis at Max-Planck-Institut für Kohlenforschung.

[1] Y.-L. Min, Y. Wan, S.-H. Yu, *Solid State Sci.* **2009**, *11*, 96–101.
[2] a) H. J. Hah, J. I. Um, S. H. Han, S. M. Koo, *Chem. Commun.* **2004**, 1012–1013; b) P. M. Arnal, M. Comotti, F. Schüth, *Angew. Chem.* **2006**, *118*, 8404–8407; *Angew. Chem. Int. Ed.* **2006**, *45*, 8224–8227; c) J. C. Park, H. J. Lee, J. Y. Kim, K. H. Park, H. Song, *J. Phys. Chem. C* **2010**, *114*, 6381–6388; d) J. C. Park, J. U. Bang, J. Lee, C. H. Ko, H. Song, *J. Mater. Chem.* **2010**, *20*, 1239–1246.
[3] Y.-L. Min, Y. Wan, R. Liu, S.-H. Yu, *Mater. Chem. Phys.* **2008**, *111*, 364–367.
[4] G. C. Bond, D. T. Thompson, *Catal. Rev. Sci. Eng.* **1999**, *41*, 319–388.
[5] M. Haruta, S. Tsubota, T. Kobayashi, H. Kageyama, M. J. Genet, B. Delmon, *J. Catal.* **1993**, *144*, 175–192.
[6] N. Lopez, T. V. W. Janssens, B. S. Clausen, M. Mavrikakis, T. Bligaard, J. K. Norskov, *J. Catal.* **2004**, *223*, 232–235.
[7] M. M. Schubert, S. Hackenberg, A. C. van Veen, M. Muhler, V. Plzak, R. J. Behm, *J. Catal.* **2001**, *197*, 113–122.
[8] A. Wittstock, B. Neumann, A. Schaefer, K. Dumbuya, C. Kübel, M. M. Biener, V. Zielasek, H.-P. Steinrück, J. M. Gottfried, J. Biener, A. Hamza, M. Bäumer, *J. Phys. Chem. C* **2009**, *113*, 5593–5600.
[9] M. Haruta, *Catal. Today* **1997**, *36*, 153–166.
[10] T. R. Ralph, M. P. Hogarth, *Platinum Met. Rev.* **2002**, *46*, 3–14.
[11] J. Y. Kim, S. B. Yoon, J. S. Yu, *Chem. Commun.* **2003**, 790–791.
[12] P. M. Arnal, F. Schüth, F. Kleitz, *Chem. Commun.* **2006**, 1203–1205.
[13] R. Güttel, M. Paul, F. Schüth, *Chem. Commun.* **2010**, *46*, 895–897.
[14] G. Büchel, K. K. Unger, A. Matsumoto, K. Tsutsumi, *Adv. Mater.* **1998**, *10*, 1036–1038.
[15] a) P. Scardi, M. Leoni, *Acta Crystallogr. Sect. A* **2002**, *58*, 190–200; b) M. Leoni, T. Confente, P. Scardi, *Z. Kristallogr. Suppl.* **2006**, *2006*, 249–254.
[16] P. M. Arnal, C. Weidenthaler, F. Schüth, *Chem. Mater.* **2006**, *18*, 2733–2739.
[17] a) J. C. Groen, J. Perez-Ramirez, *Appl. Catal. A* **2004**, *268*, 121–125; b) J. C. Groen, L. A. A. Peffer, J. Perez-Ramirez, *Microporous Mesoporous Mater.* **2003**, *60*, 1–17.

Received: January 28, 2011
Published online: June 7, 2011

